EMPIRICAL MODE DECOMPOSITION BASED INSTANTANEOUS FREQUENCY AND SEISMIC THIN-BED ANALYSIS

YANHUI ZHOU, WENCHAO CHEN, JINGHUAI GAO and YONGQIANG HE

Institute of Wave and Information, School of Electronic and Information Engineering, Xi'an Jiaotong University, 710049 Xi'an, P.R. China. zhouyh@mail.xjtu.edu.cn, wencchen@mail.xjtu.edu.cn, jhgao@mail.xjtu.edu.cn

(Received September 17, 2009; accepted January 4, 2010)

ABSTRACT

Zhou, Y., Chen, W., Gao, J. and He, Y., 2010. Empirical mode decomposition based instantaneous frequency and seismic thin-bed analysis. *Journal of Seismic Exploration*, 19: 161-172.

Empirical mode decomposition (EMD) is designed to decompose non-stationary, nonlinear data into a series of intrinsic mode functions (IMFk, k = 1,2,..., where k denotes the order of IMF) adaptively; and application of Hilbert transform to these IMFk can yield meaningful multi-component instantaneous frequency. This paper firstly applies EMD to the seismic reflection data and calculates the instantaneous frequency of IMFk. And then we employ instantaneous frequency of IMFk to analysis seismic thin bed and obtain the new insights. The results of synthetic examples show that the variation of instantaneous frequency of IMFk is more consistent with the thickness variation of thin bed, compared with that of the instantaneous frequency of original data. The channel analysis of real seismic data demonstrates that instantaneous frequency of IMFk has a significant response to the thickness variation within the channel. These studies illustrate that instantaneous frequency of IMFk can be used in qualifying seismic thin-bed thickness.

KEYWORDS: EMD, instantaneous frequency, thin bed, thickness variation, channel analysis.

INTRODUCTION

In seismic exploration, instantaneous attributes (amplitude, frequency, phase, and so on) can be used in the stratigraphic structure interpretation and lithological discrimination. By the conventional complex seismic trace analysis,

0963-0651/10/$5.00

we perform Hilbert transform on original signal and then can obtain the corresponding instantaneous attributes (Taner et al., 1979). Among these attributes, the instantaneous frequency varies with thickness and lithology variations of the layers; and especially tends to change more rapidly at the stronger reflection interface. This characteristic of instantaneous frequency makes it helpful in thin-bed analysis (Robertson and Nogami, 1984). In reality, the nonlinearity and non-stationarity of seismic signals may cause this conventional instantaneous frequency physically meaningless, such as negative value. And in addition, the reflections of several close thin beds may be composed into one reflection displayed on the seismic section. In this condition, in terms of the instantaneous frequency of the original signal, we may have difficulties in estimating the corresponding thin-bed thickness.

Hilbert-Huang Transform (HHT) can be used to analysis signal adaptively, especially applicably to non-stationary and nonlinear signal (Huang et al., 1998). Its procedure is that firstly using empirical mode decomposition (EMD) to adaptively decompose signal into a finite number of intrinsic mode functions (IMFk, k = 1,2,..., where k denotes the order of IMF) that have the characteristic of narrow-band filtering; then Hilbert transform is applied to these IMFk, and physically meaningful instantaneous frequency, and other attributes of the IMFk can be calculated. In order to clarify the writings, we define the instantaneous frequency of IMFk to be EMD based instantaneous frequency (IFPk); and define that obtained by performing Hilbert transform on original signal as no-EMD instantaneous frequency (IFP). We can notice that EMD is the main part of HHT. EMD with an alternative B-spline approach (Chen et al., 2006) has more strict mathematical foundation, and its numerical implementations demonstrate the cubic B-spline performs better than the standard cubic spline envelope approach. Based on the inherent property of complex signal, the standard EMD is extended to the complex domain (Tanaka and Mandic, 2007). And in the engineering domain, EMD and HHT are extensively implemented (Huang et al., 1999; Li and Zhang, 2006; Liang et al., 2005; Boudraa et al., 2005; Nunes et al., 2003; Zhang et al., 2006).

At the moment, the application of EMD and HHT to seismic signal processing and interpretation mainly concerns noise removal. EMD based instantaneous frequency and Hilbert amplitude spectrum of seismic data is calculated (Chagnolleau and Bananiuk, 1999). EMD and HHT are used to design filters in time and time-frequency domain to remove cable strum (Battista et al., 2007). And recently EMD is performed on seismic data in the frequency-offset domain to better attenuate coherent and random noise (Bekara and Baan, 2009).

In this paper, we mainly apply EMD-based instantaneous frequency to seismic data and examine its capabilities in seismic thin-bed analysis. We begin by delineating EMD and the EMD-based instantaneous frequency calculation.

And cubic B-spline algorithm is adopted in our EMD codes. The correlation between EMD-based instantaneous frequency and thin-bed thickness variation is demonstrated in the synthetic examples of thickness-varying multi-bed model and Marmousi2 model (Martin, 2004). Finally EMD-based instantaneous frequency is applied to 3D real seismic reflection data and is used in channel analysis.

EMD-BASED INSTANTANEOUS FREQUENCY

A. **EMD**

The objective of EMD is to decompose a signal into a series of IMFk. The IMFk satisfy two conditions: (1) the total number of extrema and that of zero crossings must differ from no more than one; (2) at any point, the average value of the local maxima envelope and the local minima envelop is equal to zero (Huang et al., 1998). Usually most of real signals are not an IMF, and we can decompose them into IMFk by sifting. The sifting process is briefly described as follows. Step 1: Regarding the original signal as initial data, we apply a cubic spline or cubic B-spline fitting to the local maxima and to local minima of the initial data, respectively; and obtain the corresponding upper envelope and lower envelope. Step 2: Subtraction of the average of the two envelops from the initial data generates a new data. Treating the obtained new data as initial data, then we repeat the sifting. Once the standard deviation (SD) between the treated initial data and corresponding new data is smaller than the predetermined value, the sifting process will be terminated and at the same time the new data is regarded as the first IMF.

We perform the process above on the difference of the original signal and the first IMF, and then can obtain the second IMF. The IMFk generation can be stopped when the difference between the original signal and the sum of generated IMFk meets the predetermined criteria. With these IMFk, the original signal s(t) can be expressed as

$$s(t) = \sum_{k=1}^{K} c_k(t) + r_K(t) \quad , \tag{1}$$

where, $c_k(t)$ denotes the obtained IMFk, K is the total number of IMFk, and $r_K(t)$ means the residue. The first IMF $c_1(t)$ contains the highest frequency components of original signal, and the last IMF $c_K(t)$ contains the lowest frequency components. In the following synthetic and real examples, we refer to Chen et al. (2006) and adopt cubic B-spline algorithm in EMD codes. And the predetermined value of SD is set as 0.05. Considering that seismic data is band-limited, we only concern the first three IMFk, k = 1,2,3.

B. **Instantaneous frequency**

In terms of the IMFk $c_k(t)$ that admit well-behaved Hilbert transform, we perform Hilbert transform on $c_k(t)$ as follows:

$$H[c_k(t)] = (1/\pi)P{\cdot}V{\cdot} \int_{-\infty}^{\infty} [c_k(t')/(t - t')]dt' \quad , \tag{2}$$

where $H[c_k(t)]$ denotes the Hilbert transform of $c_k(t)$, and $P{\cdot}V{\cdot} \int_{-\infty}^{\infty}$ means Cauchy principal value. The analytic signal $Z_k(t)$ corresponding to $c_k(t)$ can be determined as

$$Z_k(t) = c_k(t) + iH[c_k(t)] \quad , \tag{3}$$

where, $i = \sqrt{(-1)}$. The instantaneous phase $\theta_k(t)$ and frequency $\omega_k(t)$ of IMFk are derived from eq. (3) as

$$\theta_k(t) = \arctan\{H[c_k(t)]/c_k(t)\} \quad , \tag{4}$$

$$\omega_k(t) = d\theta_k(t)/dt \quad . \tag{5}$$

Eq. (5) indicates that instantaneous frequency $\omega_k(t)$ is the first derivate of instantaneous phase $\theta_k(t)$ with respect to t, which may lead to the sensitiveness of $\omega_k(t)$ to noise. In order to improve the robustness of instantaneous frequency, we replace instantaneous frequency in eq. (5) with the damped instantaneous frequency, and the corresponding expression is

$$\omega_k(t) = (1/2\pi)$$

$$[c_k(t)\{dH[c_k(t)]/dt\} - H[c_k(t)][dc_k(t)/dt]]/[e(t) + \varepsilon e_m] \quad , \tag{6}$$

where $e(t) = c_k^2(t) + H^2[c_k(t)]$, $e_m = \max[e(t)]$, and ε is a damper factor that meets $0 < \varepsilon << 1$. In the following section, both IFP and IFPk are estimated by eq. (6).

SYNTHETIC AND REAL SEISMIC DATA

A. **One-dimensional synthetic data with thickness-varying multi-bed**

We firstly evaluate EMD-based instantaneous frequency by one-dimension synthetic data. Fig. 1(a) is the model of reflection coefficient sequences and the reflection amplitude is 0.25. The (time) thickness of bed is noted by two-way

traveltime interval between two adjoining reflection interfaces in Fig. 1(a). And the main feature of the model is a gradual increase and then a gradual decrease of bed thickness. The convolution of a 45 Hz zero-phase Ricker wavelet with the reflection series in Fig. 1(a) generates the synthetic data shown in Fig. 1(b). Fig. 1(c) displays the obtained first three IMF by applying EMD to the data in Fig. 1(b). We perform Hilbert transform on synthetic data in Fig. 1(b) and on IMFk in Fig. 1(c), respectively, and then calculate the corresponding instantaneous frequency. The obtained IFP and IFPk are shown in Fig. 1(d), where IFP1 increases gradually to a peak value and then decreases gradually. We can find that the variation of IFP1 in Fig. 1(d) is consistent with that of simulated bed thickness in Fig. 1(a): the IFP1 increases with the thinning of bed

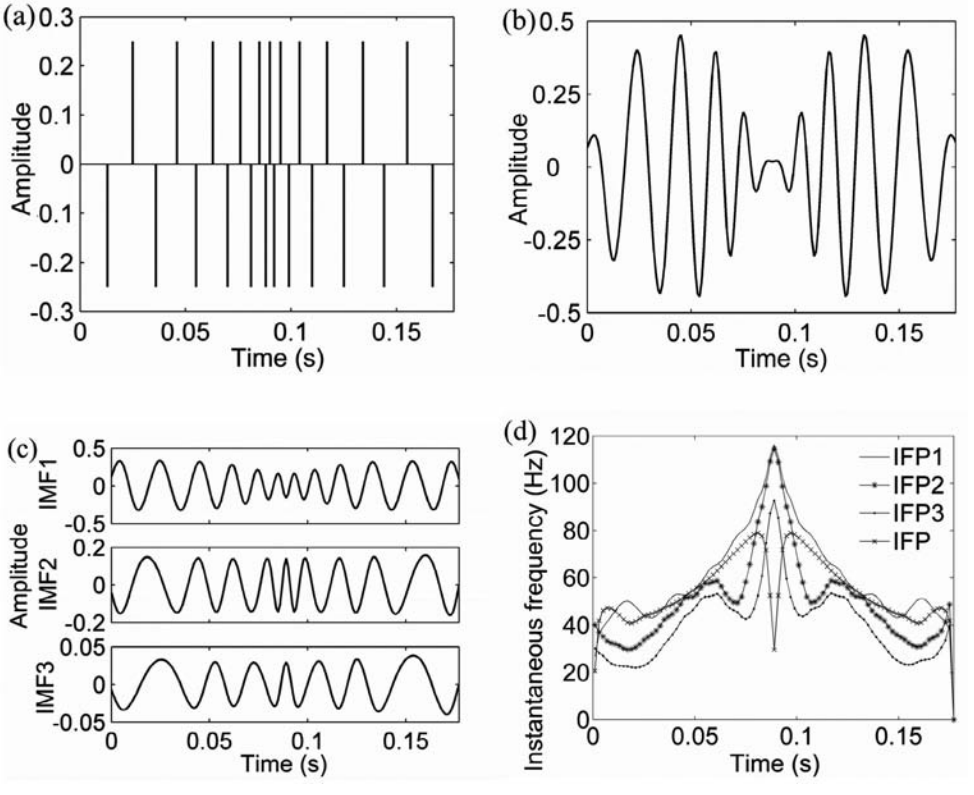

Fig. 1. Thickness-varying multi-bed model analysis: (a) equivalent-amplitude reflection series, adjacent reflection coefficients have opposite polarities, and the two-way traveltime intervals vary from 12 ms to 1 ms and then to 12 ms; (b) synthetic data, the sample rate is 1 KHz; (c) the first three IMF; (d) the instantaneous frequency of IMFk and of original signal: IFP1(solid line), IFP2 (solid line marked by star), IFP3 (solid line marked by dot), IFP (solid line marked by cross sign).

and decreases with the thickening of bed. And also, IFP2 and IFP3 have the similar variation pattern with IFP1, which can further enhance the analysis capacity of IFPk. When the bed is thick, the instantaneous frequency of original data IFP increase gradually with the thinning of bed, however, IFP falls off monotonically as the bed become thinner.

B. **Marmousi2 model and synthetic data**

The Marmousi2 model (Martin, 2004) is a complex geological model that contains many thin sandstone and shale layers. We have its P-wave velocity and wave-equation prestack depth-migration data sets available in this study [Figs. 2(a) and 2(b)]. We perform EMD on the migration result in Fig. 2(b) and obtain its first three IMFk. And then application of Hilbert transform to migration result and to its IMFk respectively generate the corresponding no-EMD instantaneous frequency IFP and EMD-based instantaneous frequency IFPk shown in Fig. 3. It should be explained that, the instantaneous frequency is referred to instantaneous wave number actually, for the migration result is displayed in depth domain. In order to consist with the results in Fig. 1, we adopt the words "instantaneous frequency" to denote instantaneous wave number in this section and the unit is cycle/km. Comparing instantaneous frequency sections in Fig. 3, we notice that IFP is marked by sharp peaks corresponding to the reflection interfaces. And IFPk is sensitive to the thickness variation of the layers: where the layer is thinner, IFPk are displayed in shades of red and are high, as the black arrows point out; where the layer is thicker, IFPk are shown in shades of blue and become lower, as the white arrows indicate.

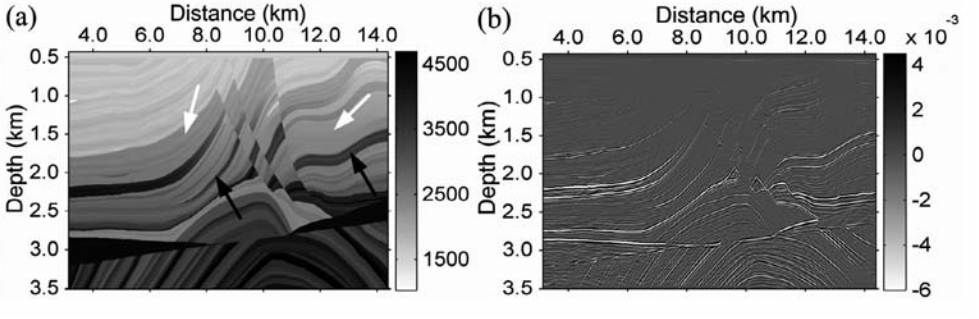

Fig. 2. Marmousi2 model: (a) P-velocity; (b) wave-equation-migrated synthetic seismic section (Martin, 2004).

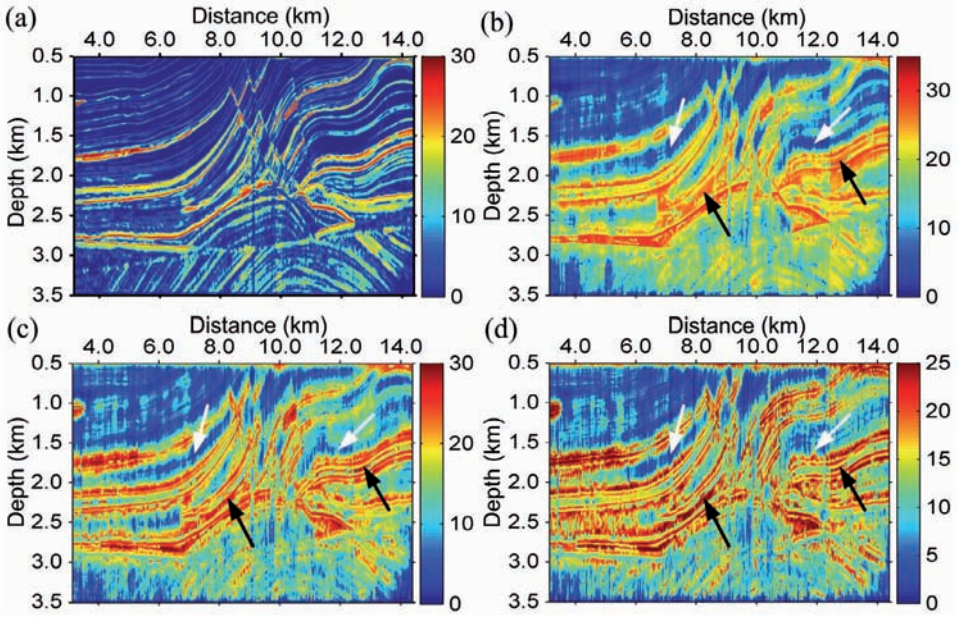

Fig. 3. Calculated the instantaneous frequency attribute from Fig. 2(b): (a) the instantaneous frequency of original data IFP; (b), (c), and (d) are the instantaneous frequency of IMF1, IMF2, and IMF3, respectively; and they are simplified as IFP1, IFP2, and IFP3. In this figure, the unit of instantaneous frequency is cycle/km.

We extract the seismic trace at the horizontal distance of 3.75 km in the Marmousi2 model, from the wave-equation prestack depth-migration data sets in Fig. 2(b) and from instantaneous frequency sections in Fig. 3, respectively. In Fig. 4 we plot IFP1 and IFP, together with the corresponding acoustic impedances and reflection coefficient sequences. Sites noted by A, B, C, D, E, F, and G in Fig. 4(b) are the locations where acoustic impedance has sharp change. In the depth intervals of AB, BC, and FG, the acoustic impedances vary little and the intervals can be regarded as the structure of thick layers; and correspondingly, IFP1 in Fig. 4(d) is shown as small value, and IFP in Fig. 4(e) only exhibit peaks in site A, B, C, F, G, and some other interfaces of acoustic impedance. In EF, the structure of reflection coefficients in Fig. 4(c) makes that EF can be treated as the composition of several thin beds, and corresponding IFP1 is high, however, IFP exhibits a rapid decrease. It can be concluded that thickness variation of layer can be revealed by IFP1 pattern: low IFP1 corresponding to thick layer, and high IFP1 corresponding to thin bed. And compared with the smoothly varying IFP1, IFP change rapidly and may aid in indicating the reflection interfaces of thick layer.

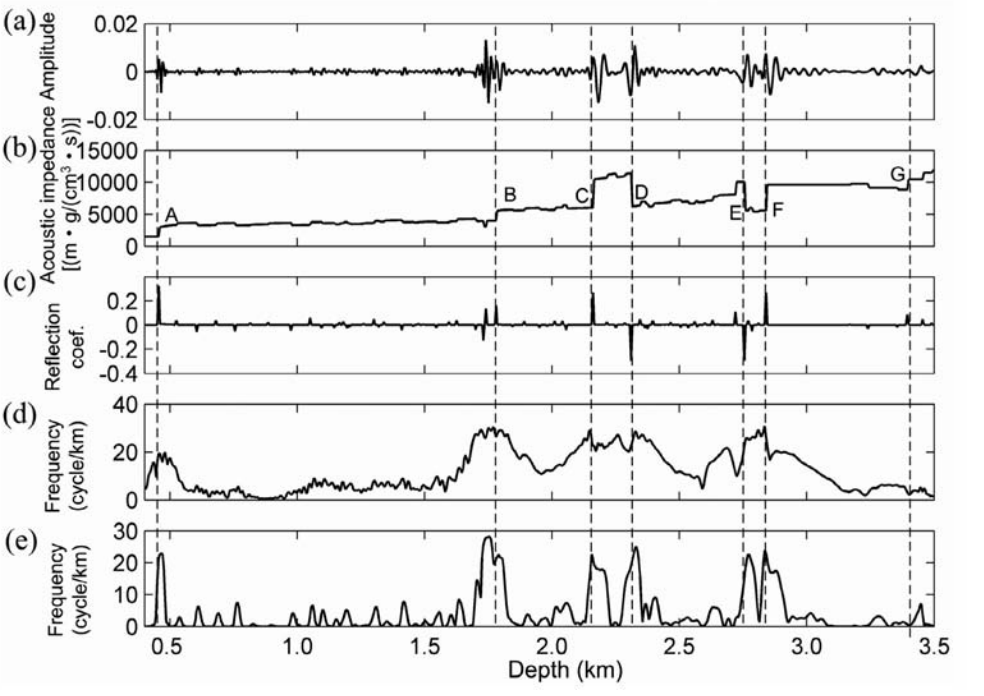

Fig. 4. Analysis of the single trace at the horizon distance of 3.75 km in the Marmousi2 model. (a) Wave-equation-migrated synthetic data; (b) the acoustic impedances; (c) the reflection coefficient series; (d) the instantaneous frequency of IMF1: IFP1; (e) the instantaneous frequency of the original trace: IFP.

C. **3D real seismic data**

In the GaoTaiZi district of Northeast China, the sandstone-filled thin bed, such as channel, is important objective in the exploration of stratigraphic hydrocarbon reservoirs. And usually seismic instantaneous attributes is used in the analysis and interpretation of thin bed. We now apply EMD to a real 3D seismic data from GaoTaiZi district, and then calculate the EMD-based and no-EMD instantaneous frequency. We extract the results along an easily-picking upper horizon of objective channels and the obtained horizon slices are shown in Fig. 5. Since IMF1 may contain more noise and the instantaneous frequency of IMF1 is less robust, we mainly concern the instantaneous frequency of IMF2 in Fig. 5(d) and no-EMD instantaneous frequency in Fig. 5(b). Wide channels C_1, C_2, C_3, and some narrow channels, are all mapped clearly in Fig. 5(b) and 5(d). In terms of the different mapping colors, the change within the channels is discernible in Fig. 5(d), however, it is not clear in Fig. 5(b), such as the features of turning channels indicated by black arrow A_1 and white arrow B_1.

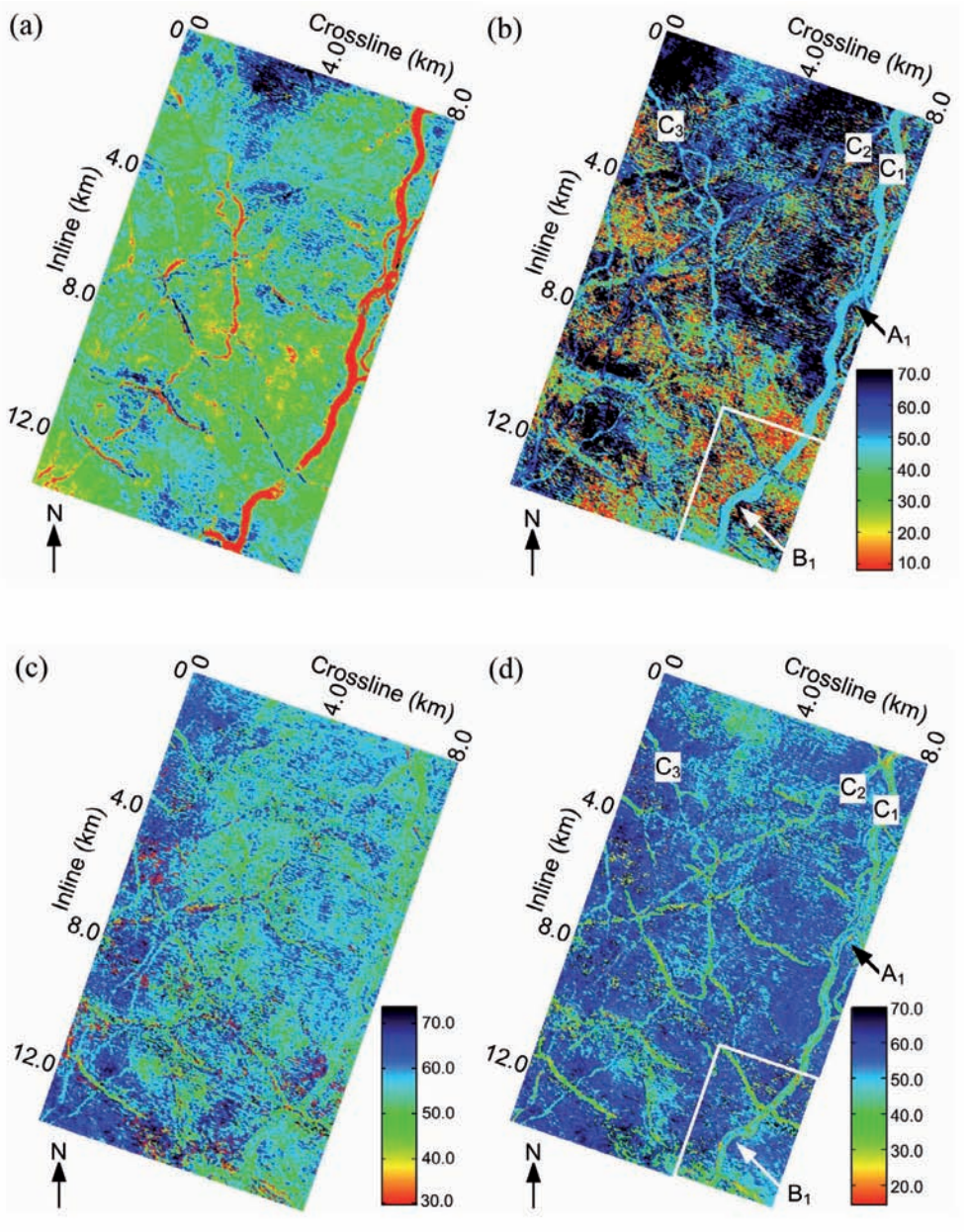

Fig. 5. The extraction map along the upper horizon of the channel from (a) the original 3D real seismic data; (b) the instantaneous frequency of original 3D seismic data; (c) the instantaneous frequency of IMF1: IFP1; (d) the instantaneous frequency of IMF2: IFP2.

In order to better delineate instantaneous frequency attribute, we amplify the maps noted by the white boxes in Fig. 5(b) and 5(d), and display them in Fig. 6. D_1D_2 and E_1E_2 cross the different parts of the channel. In order to simplify the writing, we note the part of the channel corresponding to D_1D_2 and E_1E_2 as D_3 and E_3, respectively. It is obvious that E_3 is narrower than D_3 in Fig. 6(a) and in Fig. 6(b). On the other hand, we can notice that in Fig. 6(b) D_3 is shown in shades of yellow, corresponding to a low IFP2. And E_3 is displayed in shades of blue, corresponding to a high IFP2. In term of the relationship between thickness variation of thin bed and EMD-based instantaneous frequency in Sec. III A, we can conclude that E_3 is thinner than D_3. However, in Fig. 6(a), there is little difference between the color of D_3 and the color of E_3. Fig. 6(c) and 6(d) are the original cross sections corresponding to D_1D_2 and E_1E_2, respectively. And by the channel displayed in Fig 6(c) and 6(d), we can further confirm that E_3, the part of channel that E_1E_2 crosses, is thinner and narrower than D_3, the part of channel that D_1D_2 crosses.

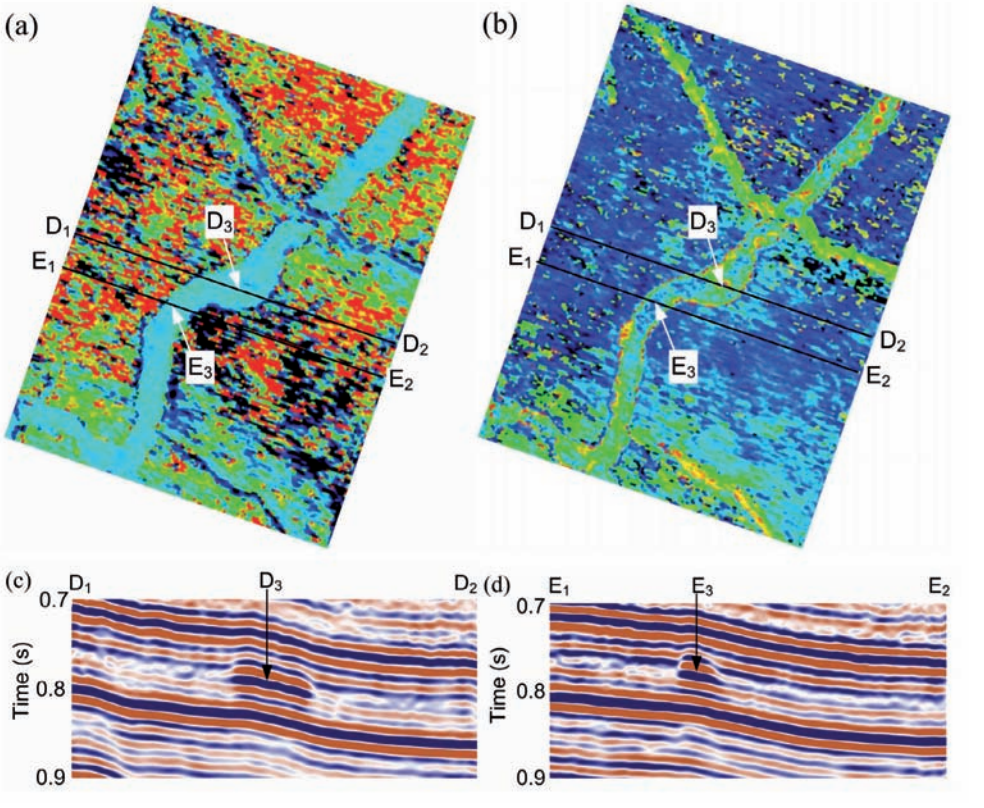

Fig. 6. The comparison of the local channel: (a) the map of white box in Fig. 5(b); (b) the map of white box in Fig. 5(d); (c) the original cross-section corresponding to D_1D_2; (d) the original cross-section corresponding to E_1E_2.

CONCLUSIONS AND DISCUSSIONS

In this paper, we calculate EMD-based instantaneous frequency IFPk of synthetic and real seismic data and apply them to the thin-bed analysis. The test of thickness-varying multi-bed model demonstrates that IFPk increases gradually with the thinning of the bed, which means that EMD based instantaneous frequency IFPk may be an indicator of thickness variation of thin bed. However, IFP decreases rapidly when the bed is thinner. The results of the complex Marmousi2 model show that the variation of EMD-based instantaneous frequency IFPk are consistent with the thickness variation of the layer. And the peak of no-EMD instantaneous frequency IFP corresponds to the reflection interface of thick layer, which may aid in detecting the reflectors. The real 3D seismic data display that when the channels become thinner, EMD-based instantaneous frequency IFP2 increases, however, the no-EMD instantaneous frequency IFP has little variation. We summarize that EMD-based instantaneous frequency IFPk has a significant response to the thickness variation of layer and can be used to qualifying the thin-bed thickness.

ACKNOWLEDGMENT

The authors thank Petrochina Daqing Oilfield Company for providing the real seismic data, and also Y. Song for his suggestions. This work was supported by the National Hi-Tech Research and Development Program of China (under grants 2006AA09A102-11) and the National Natural Science Fund of China (under grants 40730424 and 40674064).

REFERENCES

Battista, B.M., Knapp, C., Tom, M. and Vaughn, G., 2007. Application of the empirical mode decomposition and Hilbert-Huang transform to seismic reflection data. Geophysics, 72: H29-H37.

Bekara, M. and Baan, M., 2009. Random and coherent noise attenuation by empirical mode decomposition. Geophysics, 74: V89-V98.

Boudraa, A.O., Cexus, J.C. and Saidi, Z., 2005. EMD-based signal noise reduction. World Academy of Science, Engin. Technol., 2: 96-99.

Chagnolleau, I.M. and Bananiuk, R.G., 1999. Empirical mode decomposition based time-frequency attributes. Expanded Abstr., 69th Ann. Internat. SEG Mtg., Houston.

Chen, Q.H., Huang, N.E., Riemenschneider, S. and Xu, Y.S., 2006. A B-spline approach for empirical mode decompositions. Advances in Computational Mathematics, 24: 171-195.

Huang, N.E., Shen, Z., Long, R.S., Wu, M.C., Shih, H.H., Zheng, Q., Yen, N.C., Tung, C.C. and Liu, H.H., 1998. The empirical mode decomposition and the Hilbert spectrum for nonlinear and non-stationary time series analysis. Proc. Roy. Soc. Lond. A, 454: 903-995.

Huang, N.E., Shen, Z. and Long, S.R., 1999. A new view of nonlinear water waves. The Hilbert Spectrum, Ann. Rev. Fluid Mechan., 31: 417-457.

Li, H. and Zhang, Y.P, 2006. Bearing faults diagnosis based on EMD and Wigner-Ville Distribution. Abstr., 6th World Congr. Intellig. Contr. Automat. (WCICA), Dalian, China: 5447-5451.

Liang, H.L., Lin, Q.H. and Chen, J.D.Z., 2005. Application of the empirical mode decomposition to the analysis of esophageal manometric data in gastroesophageal reflux disease. IEEE Trans. Biomedical Engin., 52: 1692-1701.

Martin, G., 2004. The Marmousi2 Model, Elastic Synthetic Data, and an Analysis of Imaging and AVO in a Structurally Complex Environment. M.Sc. thesis, Univ. of Houston.

Nunes, J.C., Bouaoune, Y., Delechelle, E., Niang, O. and Bunel, Ph., 2003. Image analysis by bidimensional empirical mode decomposition. Image and Vision Computat., 21: 1019-1026.

Robertson, J.D. and Nogami, H.H., 1984. Complex seismic trace analysis of thin beds. Geophysics, 49: 344-352.

Tanaka, T. and Mandic, D.P., 2007. Complex empirical mode decomposition. IEEE Sign. Proces. Lett., 14: 101-104.

Taner, M.T., Koehler, F. and Sheriff, R.E., 1979. Complex seismic trace. Geophysics, 44, 1041-1063.

Zhang, Y.F., Gao, Y.L., Wang, L., Chen, J.H. and Shi, X.L., 2006. Application of empirical mode decomposition to remove the wall components in Doppler ultrasound signals: a simulation study. Abstr., 28th IEEE Ann. Internat. Conf. Engin. Medicine and Biol., New York: 6173-6176.